Catalysis Science & Technology

Accepted Manuscript

ROYAL SOCIETY OF CHEMISTRY

www.rsc.org/catalysis

Biogas dry reforming for syngas production: Catalytic performance of nickel supported on waste-derived SiO_2

Xuejing Chen [a], *Jianguo Jiang* [a, b, c, *], *Sicong Tian* [a], *and Kaimin Li* [a]

a. School of Environment, Tsinghua University, Beijing 100084, China

b. Key Laboratory for Solid Waste Management and Environment Safety, Ministry of Education of China

c. Collaborative Innovation Center for Regional Environmental Quality

Abstract

SiO_2 synthesized from photovoltaic waste by a vapor-phase hydrolysis method was applied as the support for a nickel catalyst in a biogas dry reforming process for the first time. The results were compared with the catalytic performance of commercial precipitated SiO_2 and ordered mesoporous SiO_2. Nickel supported on waste derived SiO_2 had a high CH_4 conversion (92.3%) and a high CO_2 conversion (95.8%) at 800°C, and there was no deactivation after 40 h-on-stream test. Catalyst characterization results revealed that the S_{BET} values and pore properties of catalysts affected the catalytic performance. A higher pore volume/S_{BET} ratio led to a smaller crystal metal size and higher metal dispersion; thus the catalyst was less prone to deactivation. This discovery will help improve catalyst design. The use of nickel supported on waste-derived SiO_2, which is competitive to commercial and mesoporous one, provides a use for photovoltaic waste as a high value-added product, and also can deliver a cheap and environmentally benign support for catalysts in the

biogas dry reforming process.

1. Introduction

Biogas is a mixture of mainly methane and carbon dioxide that is produced by the anaerobic digestion of residual biomass, such as landfilled waste, municipal sludge, and food waste. With the growing concern regarding global climate change due to anthropogenic CO_2 emissions, biogas recycling for energy-related applications has received much attention.[1] Therefore, biogas dry reforming for syngas production (Equation 1) is a recycling option with several advantages: (i) biogas dry reforming processes can simultaneously consume the two main greenhouse gases (CH_4 and CO_2); (ii) the H_2/CO ratio is close to 1, which makes it suitable for further use in the carbonylation, hydroformylation, and Fischer–Tropsch synthesis of long chain hydrocarbons;[2] and (iii) the process avoids the separation of CO_2, which is an energy intensive and costly process.[3-5]

$$CH_4 + CO_2 \leftrightarrow 2CO + 2H_2, \Delta H^0_{298K} = 247\ kJ\ \text{mol}^{-1} \quad (1)$$

The high cost and energy consumption of biogas dry reforming has restricted its industrial application.[6] Because biogas dry reforming is a strong endothermic process (see equation 1), the high reaction temperature will achieve a relatively high conversion of reactants.[7, 8] In addition, catalysts also play a vital role in the catalytic dry reforming process, which increases the cost substantially. Improving the stability and choosing relatively cheap raw materials to prepare the catalyst, without a loss in catalyst activity, is important.

The main obstacle to stability is the deactivation of catalysts, which is caused mainly by the deposition of inactive carbon and the sintering of active metal.[9, 10] To improve catalyst stability, many studies have been conducted to optimize the active metals, catalyst supports, and catalyst preparation methods.[3, 11-14] During these processes, the low-cost and availability of the raw materials used for catalyst preparation is important. Ni-based catalysts are commonly used in dry reforming process due to their reasonably good activity and low cost compared to noble metals, although they are more sensitive to coke formation than the noble metals.[2, 10, 13, 15] Many dioxides, including SiO_2[12, 16-18], ZrO_2,[19] MgO,[20] TiO_2,[8] CeO_2,[11] Al_2O_3[3, 21], and their hybrids[15, 22, 23] have been used as catalyst supports in reforming process due to their high specific surface area and high thermal stability. Of these, SiO_2 and SiO_2-based catalyst supports are the most widely used and the most promising for the industrial application of the dry reforming process due to their availability and various phase morphologies. Frontera, et al.[12] investigated the activity and stability of several nickel catalysts supported on different types of highly crystalline silica zeolites, including Ni-ITQ-6, Ni-silicalite-1, and Ni-MCM-41, and found that the heterogeneity of the support surface strongly affected the catalyst performance. Ning Wang, et al.[18] also found that the pore topology of different types of SiO_2 affected the particle dispersion, reducibility, and catalytic behavior of catalysts. The synthesis of silica zeolites consumes large amounts of organic template agents, and these zeolites are currently not commercially available in large quantities.[24] Therefore, the development of new silica materials, with a high specific surface area, high thermal

stability, and most importantly, the potential for large-scale production is essential.

In our previous study, polyporous nano-silica synthesized from photovoltaic waste $SiCl_4$ using a low temperature vapor-phase hydrolysis method (designated as SiO_2-H) was shown to have a relatively high specific surface area and high thermal stability.[25] Considering the large-scale production and poor treatment condition of photovoltaic waste $SiCl_4$, the production of SiO_2-H, and its further application as a catalyst support for biogas dry reforming represents a useful conversion of photovoltaic waste to a high value-added product, as well as providing a cheap and environmentally benign support for catalysts in the biogas dry reforming process. Using SiO_2-H as a waste-derived SiO_2 support in biogas catalytic dry reforming applications has not been reported previously.

A comprehensive evaluation of the catalytic performance of nickel supported on waste derived SiO_2 in biogas dry reforming was undertaken. SiO_2-H was used as support for nickel catalyst in a biogas dry reforming process for the first time, and commercial precipitated SiO_2 and mesoporous SiO_2 were also considered for comparison. Catalytic tests of the three different nickel supported catalysts and the related characterization of both fresh and spent catalysts were undertaken systematically.

2. Materials & Methods

2.1 Support and Catalyst Preparation

A low temperature vapor-phase hydrolysis method was used to synthesize

SiO_2-H as previously reported. [25] Silicon tetrachloride (99%: LDK Solar Ltd., Xinyu, China) was vaporized and hydrolyzed with water vapor at a temperature of 200°C, a retention time of 5 s, and a $H_2O/SiCl_4$ molar ratio of 2. Silica powder was collected and dried at 105°C for 2 h.

Commercial precipitated SiO_2 (designated as SiO_2-P) and ordered mesoporous silica (SBA-15) were purchased (Sigma–Aldrich, St Louis, MO, USA). All three of the SiO_2 supports were calcined at 700°C for 4 h to enhance their thermal stability and remove surface moisture.

An ultrasonic-assisted wetness impregnation method was used to prepare Ni/SiO_2 catalysts with a 10 wt% Ni. The metallic precursor solution was obtained by dissolving $Ni(NO_3)_2 \cdot 6H_2O$ (99%: Sigma–Aldrich) in ethanol with a Ni-ethanol ratio of 2g/L. The three SiO_2 supports were dispersed into ethanol after ultrasonic oscillation to obtain a SiO_2 colloidal solution. The Ni precursor solution was then added dropwise to the SiO_2 colloidal solution under magnetic stirring. The solution was agitated at 70°C for 12 h to remove the ethanol. The catalysts were dried at 60°C for 6 h in a vacuum oven and calcined at 800°C for 4 h. Catalysts synthesized from the SiO_2-H, SBA-15, and the SiO_2-P supports were designated Ni/SiO_2-H, Ni/SBA-15, and Ni/SiO_2-P, respectively.

2.2 Catalyst Characterization

XRD patterns were obtained with a D8 Advance X-ray diffractometer (Siemens, Munich) using Cu-Kα radiation (λ = 0.15406 nm), with a 2θ range of 0.3–80°. The Scherrer equation was used to estimate the mean Ni crystallite size based on the

diffraction peaks of the Ni (200) facet. Analysis of the Ni loading of catalysts was undertaken using an XRF analyzer (XRF-1800, Shimadzu).

Textual properties were measured by a Surface Area and Porosity Analyzer (ASAP2020 HD88, Micromeritics) through the nitrogen adsorption–desorption isotherms at 77 K. The samples were degassed at 90°C for 60 min and held at 160°C for 120 min before analysis. A Barrett–Emmett–Teller (BET) model was used to calculate the specific surface area and a Barrett-Joiner-Halenda (BJH) model was used to calculate the pore volume distribution.

Transmission electron microscopy (TEM) (JEM-2011, JEOL Ltd) was used to observe the morphology and distribution of metal sites. The samples were first dispersed in ethanol, and then one drop of ethanol solution was placed on a copper grid pre-coated with a Formvar film and dried in air. And SEM（S-5500, Hitachi）was also used to observe the morphology the samples.

The H_2 temperature-programmed reduction (H_2-TPR) was employed to analyze the reduction behavior of catalysts using a Chemisorption Analyzer (AutoChem Ⅱ 2920, Micromeritics). Catalyst samples (50 mg, 20–40 mesh) were pretreated at 400°C for 1 h under flowing Ar (30 ml/min). Upon cooling to 50°C, the sample was heated from room temperature (RT) to 1000°C with a temperature ramp of 10°C/min under a 5 vol% H_2/Ar stream (50 mL/min).

The TGA-MS method was applied to investigate the carbon deposition with a TGA/DSC 1 STARe system (METTLER TOLEDO) and a Thermostar mass spectrometer (Pfeiffer). Samples were treated at a rate of 10°C/min from RT to 900°C

under an oxygen stream of 20 mL/min with nitrogen as protection gas.

2.3 Catalytic Tests

Catalytic tests of biogas dry reforming were conducted in a fixed-bed reactor with a quartz glass tube (diameter = 6 mm) under atmospheric pressure. 200 mg of the samples (20–40 mesh) were loaded in the center of the tube reactor. Before the test, the catalysts were reduced at 800°C in situ for 1 h in a flow of 10 vol% H_2/N_2. A flow rate of 50 mL/min mixture gas (CH_4:CO_2:N_2 = 0.4:0.4:0.2) was used, in which N_2 was the reference gas for end gas analysis. The products were analyzed using on-line GC apparatus (GC-2014: Shimadzu) with a combined PC-1, MC-1, and MC-2 chromatographic column and a thermal conductivity detector. Catalytic activity of all of the samples, including a blank sample (20–40 mesh SiO_2 support without Ni) was tested at temperatures from 600 to 900°C after being in a steady state for 1 h. Stability tests of Ni/SiO_2-H, Ni/SBA-15, and Ni/SiO_2-P were conducted at 800°C for 40 h on-stream, and the products were analyzed every 30 min. The conversion (X) and the H_2/CO ratio were calculated as follows:

$$X_{CH_4}(\%) = \frac{[CH_4]_{\text{in}} - [CH_4]_{out}}{[CH_4]_{\text{in}}} \times 100$$

$$X_{CO_2}(\%) = \frac{[CO_2]_{\text{in}} - [CO_2]_{out}}{[CO_2]_{\text{in}}} \times 100$$

$$\frac{H_2}{CO}\text{ratio} = \frac{mole\ of\ H_2\ produced}{mole\ of\ CO\ produced}$$

3 Results and Discussion

3.1 Characterization of Fresh Catalysts

The XRD patterns of fresh catalysts are shown in Figure 1. Reflections of SiO_2 and NiO were detected in all three fresh SiO_2 supported nickel catalysts in their wide-angle XRD patterns (Figure 1a). Three sharp peaks were clearly visible at 37.3°, 43.3° and 62.9°, which corresponded to the crystal NiO structure for (111), (200), and (220) reflections, respectively (PDF#47-1049). Strong and broad diffractions with a wide 2θ range at 15–30° were assigned to amorphous SiO_2.[26] Compared to Ni/SiO_2-H and Ni/SiO_2-P, Ni/SBA-15 had a less erratic diffraction peak at 15–30°. This may be because SBA-15 has a highly ordered mesoporous structure. This was confirmed by the small-angle XRD patterns (Figure 1b). Ni/SBA-15 had remarkable peaks of ordered mesoporous silica (100), (110), and (200) planes, indicating a high degree of hexagonal mesoscopic organization.[27, 28] No peaks were found in the small-angle XRD patterns of Ni/SiO_2-H and Ni/SiO_2-P, indicating a heterogeneous porosity.

The average crystallite size of NiO was determined by the diffraction peak of the NiO (200) plane in XRD patterns, using the Scherrer equation (Table 1). The average crystal metal size increased in the order Ni/SiO2-P < Ni/SiO2-H < Ni/SBA-15, indicating a decreasing Ni-dispersion order Ni/SiO2-P > Ni/SiO2-H > Ni/SBA-15.[26, 29] The BET specific surface area (S_{BET}) value and pore properties of catalyst supports and freshly prepared catalysts are shown in Table S1. After impregnation, the S_{BET} value and pore volume decreased in all three of the catalysts. This phenomenon might be caused by pore blocking during the impregnation process. The S_{BET}, pore volume, average pore size, and average Ni-loading of freshly prepared catalysts are also presented in Table 1. The largest pore volume and largest average pore size were

found in Ni/SiO_2-P, while Ni/SBA-15 had the largest S_{BET} value. There was no obvious connection between the S_{BET} value and pore volume of catalysts, but the pore volume/S_{BET} ratio decreased in the order Ni/SiO2-P > Ni/SiO2-H > Ni/SBA-15, which was in accordance with the Ni-dispersion order, and Bappy Saha[30] also proved that a high pore volume/S_{BET} ratio contributes to high catalytic performance. The XRF results in Table 1 show that the Ni-loading was slightly higher than the set value of 10 wt%. This might be caused by weight loss during the pre-calcination of the supports, resulting in a higher Ni content in the catalysts.

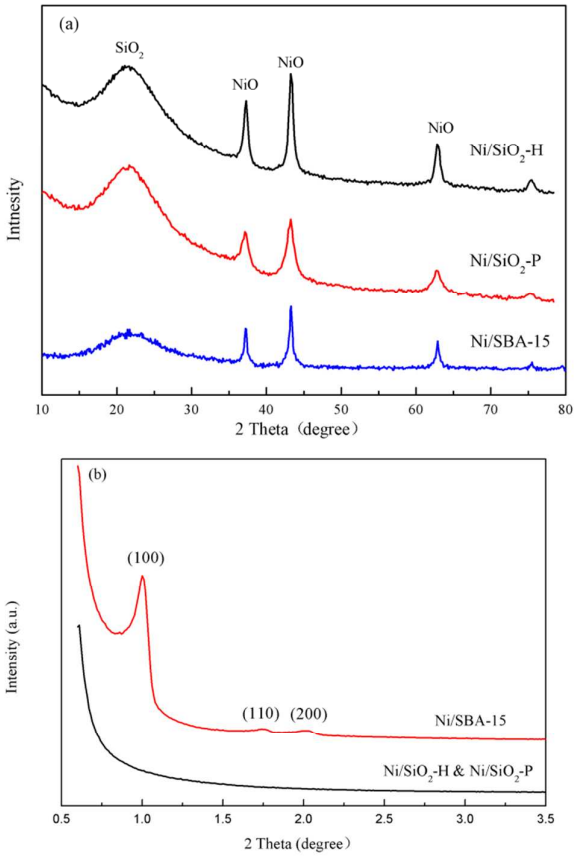

Figure 1. XRD patterns of fresh 10% Ni/SiO_2 catalysts (before reduction). (a) Wide-angle XRD patterns, (b) small-angle XRD patterns.

Table 1. The main textural properties of fresh catalysts.

Catalysts	Ni loading [a] wt. (%)	Average crystal size [b] nm	S_{BET} [c] m^2/g	Pore volume cm^3/g	Average pore size Å	Pore volume to S_{BET} ratio 10^{-9} m
Ni/SiO_2-H	10.55	8.38	153	0.40	107	2.6
Ni/SBA-15	10.90	10.23	332	0.42	50	1.3
Ni/SiO_2-P	10.15	6.25	279	0.88	126	3.2

a Determined by the XRF method.

b Determined by the Scherrer equation from the Ni (200) plane of XRD.

c. Specific surface area calculated by BET method.

SEM images of the three supports were shows in Figure S1. From the SEM images of supports, we can see that both SiO_2-H and SiO_2-P have a loose and porous structure with a non-uniform pore size, while SBA-15 have an uniform cylindrical pores. TEM images of fresh catalysts are shown in Figure 2. The translucent particles with an irregular shape are supports of Ni/SiO_2-H and Ni/SiO_2-P catalysts (Figure 2a and 2b),[25] and crystal NiO particles were uniformly supported on SiO_2-H and SiO_2-P. In contrast, Ni/SiO_2-P had a smaller NiO particle size and greater homogeneity in metal dispersion. In Figure 2c and 2d, a two-dimensional hexagonal texture is assigned to SBA-15.[15, 31] The pores of Ni/SBA-15 were of a uniform size of ~5 nm (Figure S2), which is also confirmed by the BET results in Table 1. Some NiO particles were uniformly loaded on the outside surface of SBA-15, which differed

184 greatly from the crystallite sites inside the porous structure. The regulated growth of
185 crystals inside the narrowly distributed channels might have been responsible for the
186 difference in NiO particle size, resulting in less homogeneity of NiO particles than in
187 Ni/SiO_2-P and Ni/SiO_2-H. The particle size of supported NiO increased in the order of
188 Ni/SiO_2-P < Ni/SiO_2-H < Ni/SBA-15, which was in agreement with the Scherrer
189 equation results.

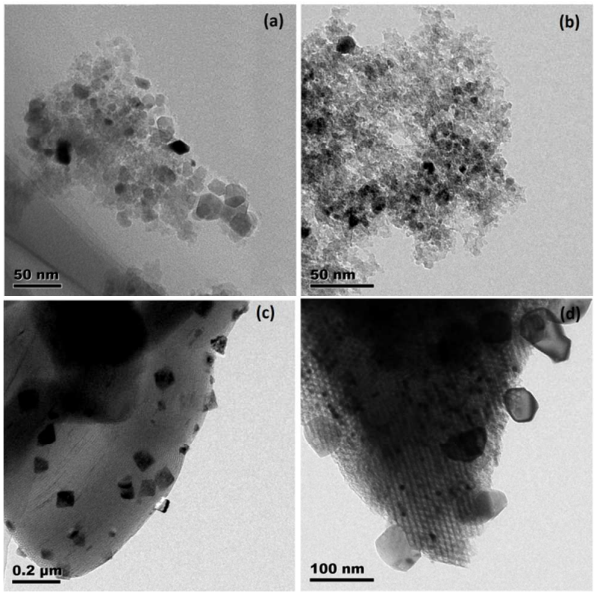

Figure 2. TEM images of fresh catalysts (before reduction): (a) Ni/SiO_2-H, (b) Ni/SiO_2-P, (c) and (d) Ni/SBA-15.

190 The reducibility and different Ni species in the SiO_2 supported nickel catalysts
191 were investigated using H_2-TPR (Figure 3). All of the catalysts had a broad and
192 overlapping H_2 consumption peak from 300 to 800°C, indicating the presence of
193 nickel oxides that had different interactions with the supports.[16,32] The highest H_2
194 reduction temperature of Ni/SiO_2-H, Ni/SBA-15, and Ni/SiO_2-P was 680°C, 700°C,

and 750°C, respectively, in the order Ni/SiO_2-H < Ni/SBA-15 < Ni/SiO_2-P, suggesting an enhancement of NiO-SiO interactions.[26, 33] In addition, two separate reduction regions can be seen in the Ni/SBA-15 catalyst; i.e., the broad peak at 430°C and the shoulder peak around 620°C. These peaks might relate to the reduction of NiO particles supported on the outside surface and inside the porous structure of SBA-15, respectively, which can also be clearly distinguished in the TEM results. The H_2-TPR profiles also confirmed that 800°C was the appropriate pre-reduction temperature for the reduction of reducible catalysts.

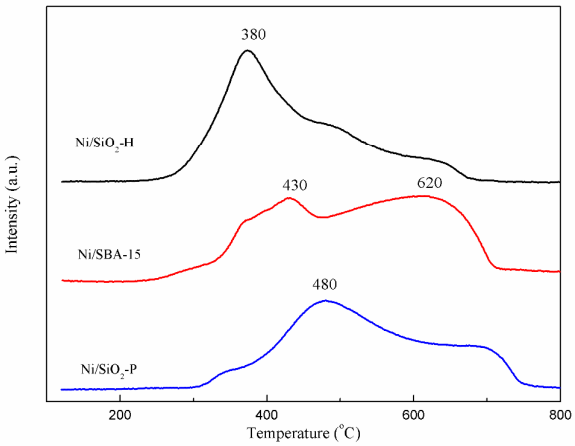

Figure 3. H_2-TPR profiles of Ni/SiO_2 catalysts (reduced in a 5 vol% H_2/Ar stream at a temperature ramp of 10°C/min).

3.2 Catalytic Performance in Biogas Reforming

Effect of temperature

The dry reforming activity of catalysts is indicated by the conversion of CH_4 and CO_2, and the selectivity is expressed in terms of the H_2/CO ratio. Figure 4 shows the activity and selectivity results for all the three types of SiO_2 supported nickel catalysts

from 600 to 900°C. Generally, the conversion of both CH_4 and CO_2 increased as the temperature increased from 600 to 900°C. This may be because the dry reforming reaction of biogas is a strong endothermic reaction (Equation 1), and a higher temperature will increase the conversion rate, as observed in earlier studies.[6, 7, 34] Of the different catalysts, the CH_4 conversion of Ni/SiO_2-H was the highest during the whole temperature range, and when the temperature was higher than 650°C, the CH_4 conversion of Ni/SiO_2-P was slightly higher than that of Ni/SBA-15. As the temperature increasing, less difference was observed in the CO_2 conversion between different catalysts. Taking Ni/SiO_2-H as an example, the CH_4 conversion increased from 55% to 98% and the CO_2 conversion increased from 52% to 98% when temperature increased from 600 to 900°C. When the temperature was 800°C, both CH_4 and CO_2 conversion exceeded 90%. There is only slight increase in CH_4 and CO_2 conversions at temperatures >800 ºC

The H_2/CO ratio of different catalysts at various temperatures is shown in Figure 4c. When the temperature was higher than 650°C, the H_2/CO ratio of all samples was < 1. The reverse water-gas-shift reaction (RWGS, Equation 2) can consume the additional H_2 and produces CO, which lowers the H_2/CO ratio.[9] When the temperature was < 850°C, the H_2/CO ratio of Ni/SiO_2-H was slightly higher than that of Ni/SBA-15 and Ni/SiO2-P, indicating a smaller contribution from the RWGS reaction.

$$CO_2 + H_2 \leftrightarrow CO + H_2O, \Delta H^0_{298K} = 41\ kJ\ \text{mol}^{-1} \quad (2)$$

$$CH_4 \leftrightarrow C + 2H_2, \Delta H^0_{298K} = 75\ kJ\ \text{mol}^{-1} \quad (3)$$

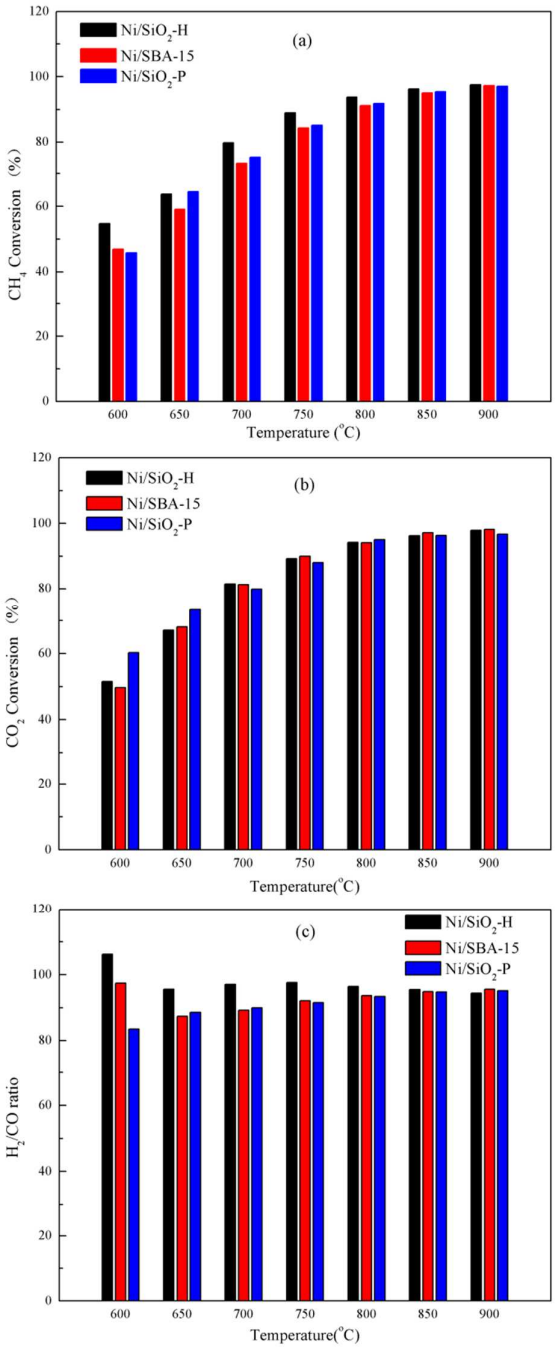

Figure 4. The influence of temperature on the catalytic activity of Ni/SiO_2 catalysts: (a) CH_4 conversion, (b) CO_2 conversion, and (c) H_2/CO ratio. (GHSV = 15 000 $mL \bullet g_{cat}^{-1} \bullet h^{-1}$, atmospheric pressure)

229 **Stability tests**

Temperature tests indicated that at 800°C, both CH_4 and CO_2 conversion was high (> 90%). Blank tests showed that when the temperature was higher than 750°C, H_2 and CO was detected in the outlet gas (Figure S3), which might be caused by RWGS reaction (Equation 2) and methane decomposition reaction (Equation 3). Therefore, 800°C was chosen as the appropriate temperature to conduct stability tests. Figure 5 shows the 40-h-on-stream catalyst test results for all catalyst samples at 800°C. All three of the samples showed good stability during the 40 h on-stream, and no decay of activity was found in all samples. The conversion of CH_4 was slightly lower than the conversion of CO_2 and the H_2/CO ratio was < 1.

The average CH_4 conversion, CO_2 conversion, and H_2/CO ratio are summarized in Table 2. The average CH_4 conversion increased in the order Ni/SBA-15 < Ni/SiO2-P < Ni/SiO2-H, and the average CO_2 conversion increased in the order Ni/SBA-15 < Ni/SiO_2-H < Ni/SiO_2-P. The contribution of the RWGS reaction increased the conversion of CO_2 and decreased the H_2/CO ratio. The higher the degree of the reverse water gas shift reaction process, the larger the difference between CH_4 and CO_2 conversion, and the lower the H_2/CO ratio. These theoretical considerations are confirmed by the actual test results shown in Table 2. The highest average H_2/CO ratio of Ni/SiO_2-H indicated that the secondary reaction was minimized to a greater extent than in Ni/SBA-15 and Ni/SiO_2-P.

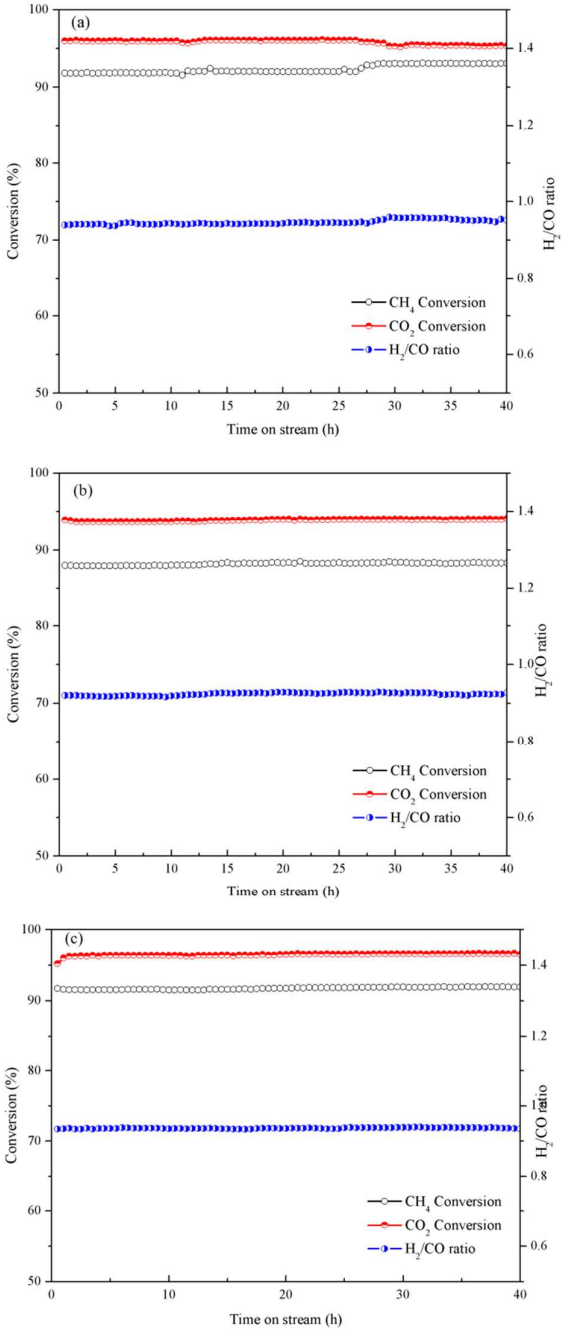

Figure 5. Stability tests of Ni/SiO_2 catalysts under 800°C for 40 h: (a) Ni/SiO_2-H, (b) Ni/SBA-15, and (c) Ni/SiO_2-P. (GHSV = 15 000 $mL \bullet g_{cat}^{-1} \bullet h^{-1}$, atmospheric pressure)

Table 2. Average catalytic activity of all three of the catalyst samples during 40 h-on-stream.

Catalysts	Average CH_4 conversion (%)	Average CO_2 conversion (%)	Conversion difference (%)	Average H_2/CO ratio
Ni/SiO_2-H	92.3	95.8	3.5	0.946
Ni/SBA-15	88.2	93.9	5.7	0.924
Ni/SiO_2-P	91.8	96.5	4.7	0.937

3.3 Post-reaction Characterization.

Figure 6 shows the N_2 adsorption-desorption isotherms and BJH desorption pore size distribution analysis of fresh and spent catalysts. The N_2 adsorption-desorption isotherms of both fresh and spent Ni/SiO_2-H (Figure 6a) and Ni/SiO_2-P (Figure 6c) catalysts displayed an approximate type IV isotherm as defined by the International Union of Pure and Applied Chemistry (IUPAC). The presence of a type H3 hysteresis loop indicates the existence of mesopores, and the unlimited adsorption at high P/P_0 values suggests that aggregates of plate-like particles give rise to slit-shaped pores. [24, 35] The results were also confirmed by Figures 2a and 2b. The N_2 adsorption-desorption isotherms of both fresh and spent Ni/SBA-15 (Figure 6b) catalysts displayed a typical Type IV isotherm and a standard H1 type hysteresis loop as defined by the IUPAC, and were characteristic of mesoporous materials with highly uniform cylindrical pores,[27] which also supports the XRD and TEM results. The fresh Ni/SiO_2-H and Ni/SiO_2-P catalysts had a wide BJH desorption pore size distribution, while fresh Ni/SBA-15 had a highly narrow size distribution with a mean diameter of 5.0 nm, which was in accordance with the HR-TEM results (Figure S2).

After the 40-h-on-stream tests, there was a decrease in the BET surface area and pore volume, and an increase in average pore size in all of the spent catalysts (see Table S1). This agreed with the BET analysis results for Ni/γ-Al_2O_3 reported by Srinivas Appari.[36] The catalytic reaction process did not change the shape of the N_2 adsorption-desorption isotherms of Ni/SiO_2-H and Ni/SBA-15, or their BJH desorption pore size distribution, and only a slight change in the average pore size was observed due to a slight blocking phenomenon. There was a difference in the hysteresis loop for Ni/SiO_2-P between fresh and spent catalysts. The shifting of the relative pressure of the hysteresis loop to a higher value was observed, leading to an obvious change in the BJH desorption pore size distribution, with the average pore size shifted greatly from 126 to 270 nm. According to Aziza[27], the hysteresis loops at lower and higher relative pressures represent the intra- and inter- particle porosity, respectively. There might be a decrease in intra-particle porosity and an increase in the inter-particle porosity of Ni/SiO_2-P after a stability test, therefore the decrease of smaller pore size due to intra-particle porosity may result in an increase in the average pore size.

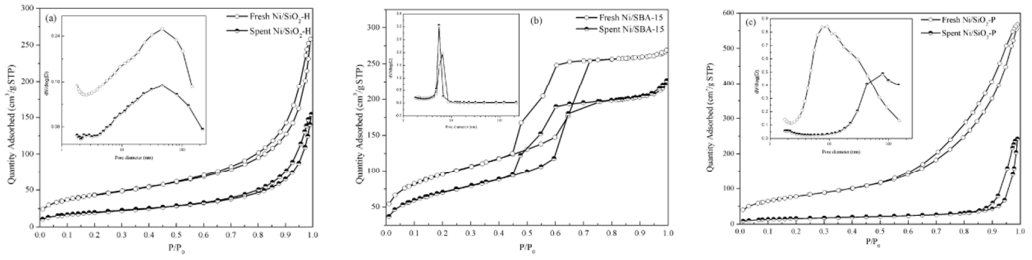

Figure 6. N_2 adsorption-desorption isotherms and the BJH desorption pore size distribution for fresh and spent catalysts: (a) Ni/SiO_2-H, (b) Ni/SBA-15, and (c) Ni/SiO_2-P. The inset shows the pore size distribution.

Figure 7 shows TEM images of spent catalysts. The original structure of all catalysts was maintained after 40-h-on-stream tests. Spent Ni/SiO_2-H and Ni/SiO_2-P catalysts kept their amorphous structure, and Ni/SBA-15 kept its two-dimensional hexagonal texture. However, there was an obvious pore size increase in the spent Ni/SiO_2-P catalyst (Figure 7b), which was supported by the BJH pore size distribution results shown in Figure 6c. A slight metal agglomeration phenomenon was observed in spent Ni/SiO_2-H and Ni/SiO_2-P catalysts (Figures 7a and 7b). The two-dimensional hexagonal channel of spent Ni/SBA-15 limited the agglomeration of active metals inside the pore (Figure 7c), while the active metals supported on the outside surface experienced significant agglomeration, and even detached from the SBA-15 support (Figure 7d). Ilenia Rossetti, et al. also reported that large particles exposed a small interface with the support surface, which led to a weaker interaction, thus, easy to detach from the support.[26] No carbon was found in any of the three spent catalysts, indicating negligible coke deposition.

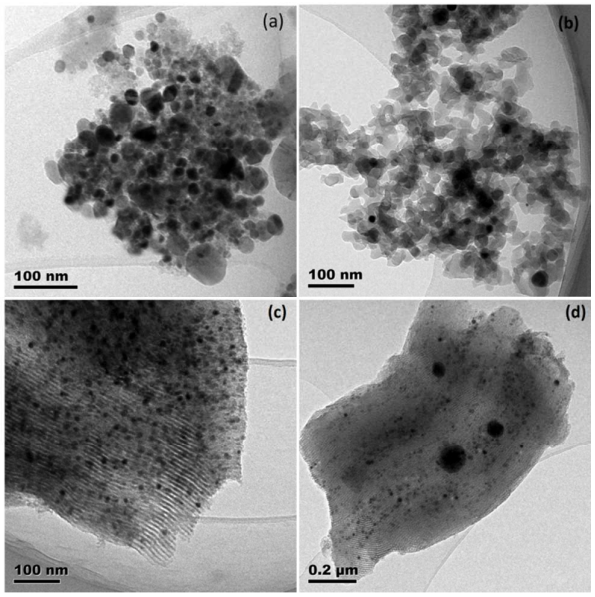

Figure 7. TEM images of spent catalysts: (a) Ni/SiO_2-H, (b) Ni/SiO_2-P, (c) and (d) Ni/SBA-15.

295 The results of the TGA-MS analysis of the spent catalysts are shown in Figure 8.
296 The thermo-grams can be divided into two different temperature regions (Figure 8a).
297 All of the spent catalysts experienced an increase in weight at low temperature ranges
298 and a decrease in weight at high temperature ranges. The oxidation of nickel particles
299 at temperatures above 200°C caused the weight increase, and the 3% weight increase
300 of spent catalysts was inconsistent with the theoretical weight increase of 10% due to
301 nickel particle oxidation, which was also reported by Jianqiang Zhu[17]. Weight loss at
302 temperatures above 400°C was ascribed to the oxidation of deposited carbon. [37] CO_2
303 MS signals from TPO process of three spent catalysts were shown in Figure 8b. Since
304 O_2 was used as react gas and N_2 was used as protection gas, the signal of molecular
305 weight at 44 was only supposed to be CO_2, which was generated by the oxidation of

306 deposited carbon. The CO_2 generation peak range of spent Ni/SiO_2-H, Ni/SBA-15,
307 and Ni/SiO_2-P were 450-700°C, 500-700°C, and 580-700°C, respectively,
308 corresponding to the weight loss temperature ranges of the three catalysts. Although
309 MS is a semi-quantitative method, we can still distinguish that a higher weight loss
310 amount of TGA resulted in a higher MS signal intensity. So a very weak CO_2 signal
311 intensity of spent Ni/SiO_2-P implied its lowest carbon deposition. The amount of coke
312 deposited on spent Ni/SiO_2-H, Ni/SBA-15, and Ni/SiO_2-P catalysts was calculated to
313 be 2.1, 2.7 , and 0.3 wt.%, respectively, which was in the low range of carbon
314 deposited (0.89–6.56 wt.%) on Ni/SiO_2 catalysts after a 30-h test, as reported by
315 Zhu.[17] In conclusion, the results showed that little coke was deposited on the catalysts,
316 and the formation of coke was related to the metal dispersion of the catalysts. The
317 smaller crystal size of metal catalysts will lead to a catalyst that is less prone to
318 deactivation.

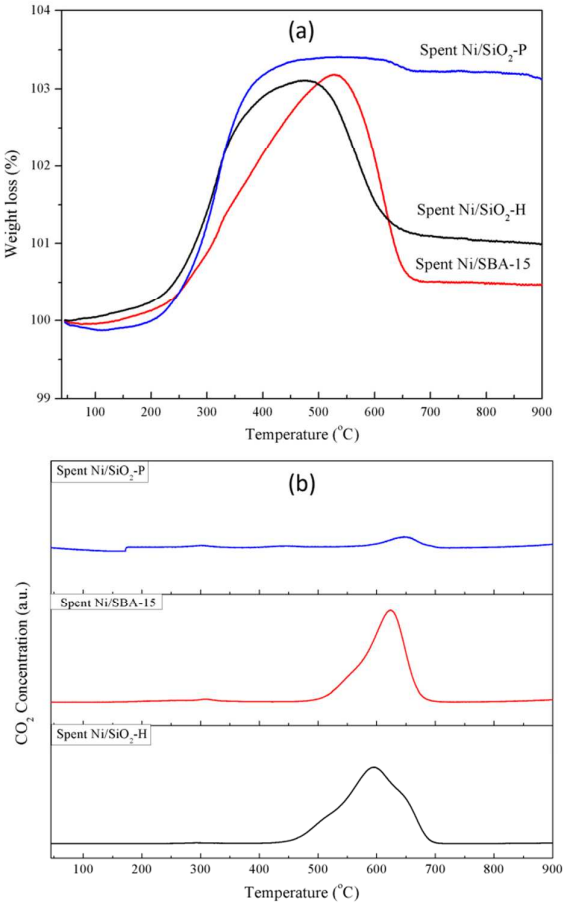

Figure 8. (a) TGA profiles of spent Ni/SiO_2 catalysts, (b) MS signals of CO_2 (20 mL/min O_2 stream under a temperature ramp of 10°C/min with N_2 as protection gas).

4 Conclusions

In summary, Waste-derived SiO_2 obtained from photovoltaic waste $SiCl_4$ by a vapor-phase hydrolysis method was applied as the support for a nickel catalyst in a biogas dry reforming process for the first time. Catalytic tests results showed that the conversion of CH_4 and CO_2 increased as temperature increased from 600 to 900°C. When temperature was 800°C, it reached a high CH_4 conversion (92.3%) and a high CO_2 conversion (95.8%), and there was no deactivation after 40 h-on-stream test.

Compared to commercial precipitated SiO_2 and ordered mesoporous SiO_2, the catalytic activity of waste-derived SiO_2 is equivalent to those of commercial precipitated SiO_2, and even superior to those of mesoporous SiO_2. The coke deposition amount after stability tests follows the order commercial precipitated SiO_2 < waste-derived SiO_2 < mesoporous SiO_2. It is further demonstrated that coke deposition in biogas dry reforming process is related to the textual properities of catalysts. A higher pore volume/S_{BET} ratio will lead to a smaller crystal metal size and higher metal dispersion; thus the catalyst is less prone to deactivation. This discovery will help improve catalyst design.

In conclusion, waste-derived SiO_2 used as catalyst support in biogas dry reforming process shows a high catalytic activity and good stability, which is competitive to commercial and mesoporous one. Considering the large-scale production and poor treatment condition of photovoltaic waste $SiCl_4$, the production of waste-derived SiO_2, and its further application as a catalyst support for biogas dry reforming represents a useful conversion of photovoltaic waste to a high value-added product, as well as providing a cheap and environmentally benign support for catalysts in the biogas dry reforming process.

ASSOCIATED CONTENT

Supporting Information

Supplementary materials for online publication are available via the Internet at http://pubs.rsc.org.

AUTHOR INFORMATION

Corresponding Author

*Phone: 86-10-62783548; fax: 86-10-62783548;

e-mail: jianguoj@mail.tsinghua.edu.cn.

Notes

The authors declare no competing financial interest.

ACKNOWLEDGMENTS

The authors gratefully acknowledge the Hi-Tech Research and Development Program (863) of China for financial support (Grant No. 20121868156).

REFERENCES

1. Budzianowski, W. M., Negative carbon intensity of renewable energy technologies involving biomass or carbon dioxide as inputs. *Renew. Sust. Energ. Rev.* **2012,** *16*, (9), 6507-6521.

2. Corthals, S.; Van Nederkassel, J.; De Winne, H.; Geboers, J.; Jacobs, P.; Sels, B., Design of active and stable $NiCeO_2ZrO_2MgAl_2O_4$ dry reforming catalysts. *Appl. Catal. B-Environ.* **2011,** *105*, (3-4), 263-275.

3. Ewbank, J. L.; Kovarik, L.; Kenvin, C. C.; Sievers, C., Effect of preparation methods on the performance of Co/Al_2O_3 catalysts for dry reforming of methane. *Green Chem.* **2014,** *16*, (2), 885.

4. Broda, M.; Manovic, V.; Imtiaz, Q.; Kierzkowska, A. M.; Anthony, E. J.; Muller, C. R., High-purity hydrogen via the sorption-enhanced steam methane reforming reaction over a synthetic CaO-based sorbent and a Ni catalyst. *Environ. Sci. Technol.* **2013,** *47*, (11), 6007-14.

5. Chaemchuen, S.; Kabir, N. A.; Zhou, K.; Verpoort, F., Metal-organic frameworks for upgrading biogas via CO_2 adsorption to biogas green energy. *Chem. Soc. Rev.* **2013,** *42*, (24),

9304-32.

6. Kathiraser, Y.; Wang, Z.; Kawi, S., Oxidative CO_2 reforming of methane in $La_{0.6}Sr_{0.4}Co_{0.8}Ga_{0.2}O_3$-delta (LSCG) hollow fiber membrane reactor. *Environ. Sci. Technol.* **2013,** *47*, (24), 14510-7.

7. Serrano-Lotina, A.; Daza, L., Influence of the operating parameters over dry reforming of methane to syngas. *Int. J. Hydrogen Energ.* **2014,** *39*, (8), 4089-4094.

8. Shinde, V. M.; Madras, G., Catalytic performance of highly dispersed Ni/TiO_2 for dry and steam reforming of methane. *RSC Adv.* **2014,** *4*, (10), 4817.

9. Serrano-Lotina, A.; Daza, L., Highly stable and active catalyst for hydrogen production from biogas. *J. Power Sources* **2013,** *238*, 81-86.

10. Taufiq-Yap, Y. H.; Sudarno; Rashid, U.; Zainal, Z., CeO_2–SiO_2 supported nickel catalysts for dry reforming of methane toward syngas production. *Appl. Catal. A-Gen.* **2013,** *468*, 359-369.

11. Derk, A. R.; Moore, G. M.; Sharma, S.; McFarland, E. W.; Metiu, H., Catalytic Dry Reforming of Methane on Ruthenium-Doped Ceria and Ruthenium Supported on Ceria. *Top Catal.* **2013,** *57*, (1-4), 118-124.

12. Frontera, P.; Macario, A.; Aloise, A.; Antonucci, P. L.; Giordano, G.; Nagy, J. B., Effect of support surface on methane dry-reforming catalyst preparation. *Catal. Today* **2013,** *218-219*, 18-29.

13. Luengnaruemitchai, A.; Kaengsilalai, A., Activity of different zeolite-supported Ni catalysts for methane reforming with carbon dioxide. *Chem. Eng. J.* **2008,** *144*, (1), 96-102.

14. Kim, H. Y.; Park, J. N.; Henkelman, G.; Kim, J. M., Design of a highly nanodispersed Pd-MgO/SiO_2 composite catalyst with multifunctional activity for CH_4 reforming. *ChemSusChem* **2012,** *5*, (8), 1474-81.

15. Zuo, Z.-J.; Shen, C.-F.; Tan, P.-J.; Huang, W., Ni based on dual-support Mg-Al mixed oxides and SBA-15 catalysts for dry reforming of methane. *Catal. Commun.* **2013,** *41*, 132-135.

16. Zhu, J.; Peng, X.; Yao, L.; Tong, D.; Hu, C., CO_2 reforming of methane over Mg-promoted Ni/SiO_2 catalysts: the influence of Mg precursors and impregnation sequences. *Catal. Sci. Technol.* **2012,** *2*, (3), 529.

17. Zhu, J.; Peng, X.; Yao, L.; Shen, J.; Tong, D.; Hu, C., The promoting effect of La, Mg, Co and Zn on the activity and stability of Ni/SiO_2 catalyst for CO_2 reforming of methane. *Int. J.*

Hydrogen Energ. **2011,** *36*, (12), 7094-7104.

18. Wang, N.; Yu, X.; Wang, Y.; Chu, W.; Liu, M., A comparison study on methane dry reforming with carbon dioxide over $LaNiO_3$ perovskite catalysts supported on mesoporous SBA-15, MCM-41 and silica carrier. *Catal. Today* **2013,** *212*, 98-107.

19. Rossetti, I.; Lasso, J.; Nichele, V.; Signoretto, M.; Finocchio, E.; Ramis, G.; Di Michele, A., Silica and zirconia supported catalysts for the low-temperature ethanol steam reforming. *Appl. Catal. B-Environ.* **2014,** *150-151*, 257-267.

20. Danilova, M. M.; Fedorova, Z. A.; Zaikovskii, V. I.; Porsin, A. V.; Kirillov, V. A.; Krieger, T. A., Porous nickel-based catalysts for combined steam and carbon dioxide reforming of methane. *Appl. Catal. B-Environ.* **2014,** *147*, 858-863.

21. Zhang, X.; Wang, N.; Xu, Y.; Yin, Y.; Shang, S., A novel Ni–Mg–Al-LDHs/γ-Al_2O_3 Catalyst Prepared by in-situ synthesis method for CO_2 reforming of CH_4. *Catal. Commun.* **2014,** *45*, 11-15.

22. Djinović, P.; Osojnik Črnivec, I. G.; Erjavec, B.; Pintar, A., Influence of active metal loading and oxygen mobility on coke-free dry reforming of Ni–Co bimetallic catalysts. *Appl. Catal. B-Environ.* **2012,** *125*, 259-270.

23. Kim, D. H.; Seo, H. O.; Jeong, M.-G.; Kim, Y. D., Reactivity and Stability of Ni Nanoparticles Supported by Mesoporous SiO_2 and TiO_2/SiO_2 for CO_2 Reforming of CH_4. *Catal. Lett* **2013,** *144*, (1), 56-61.

24. Goeppert, A.; Meth, S.; Prakash, G. K. S.; Olah, G. A., Nanostructured silica as a support for regenerable high-capacity organoamine-based CO_2 sorbents. *Energy Environ. Sci.* **2010,** *3*, (12), 1949.

25. Chen, X.; Jiang, J.; Yan, F.; Tian, S.; Li, K., A novel low temperature vapor phase hydrolysis method for the production of nano-structured silica materials using silicon tetrachloride. *RSC Adv.* **2014,** *4*, (17), 8703.

26. Rossetti, I.; Gallo, A.; Dal Santo, V.; Bianchi, C. L.; Nichele, V.; Signoretto, M.; Finocchio, E.; Ramis, G.; Di Michele, A., Nickel Catalysts Supported Over TiO_2, SiO_2 and ZrO_2 for the Steam Reforming of Glycerol. *ChemCatChem* **2013,** *5*, (1), 294-306.

27. Aziz, M. A. A.; Jalil, A. A.; Triwahyono, S.; Mukti, R. R.; Taufiq-Yap, Y. H.; Sazegar, M. R., Highly active Ni-promoted mesostructured silica nanoparticles for CO_2 methanation. *Appl. Catal. B-Environ.* **2014,** *147*, 359-368.

28. Zhao, M.; Church, T. L.; Harris, A. T., SBA-15 supported Ni-Co bimetallic catalysts for enhanced hydrogen production during cellulose decomposition. *Appl. Catal. B-Environ.* **2011,** *101*, (3-4), 522-530.

29. Wang, X.; Meng, L.; Wu, F.; Jiang, Y.; Wang, L.; Mu, X., Efficient conversion of microcrystalline cellulose to 1,2-alkanediols over supported Ni catalysts. *Green Chem.* **2012,** *14*, (3), 758.

30. Saha, B.; Khan, A.; Ibrahim, H.; Idem, R., Evaluating the performance of non-precious metal based catalysts for sulfur-tolerance during the dry reforming of biogas. *Fuel* **2014,** *120*, 202-217.

31. Qian, L.; Ma, Z.; Ren, Y.; Shi, H.; Yue, B.; Feng, S.; Shen, J.; Xie, S., Investigation of La promotion mechanism on Ni/SBA-15 catalysts in CH_4 reforming with CO_2. *Fuel* **2014,** *122*, 47-53.

32. Pompeo, F.; Santori, G. F.; Nichio, N. N., Hydrogen production by glycerol steam reforming with Pt/SiO_2 and Ni/SiO_2 catalysts. *Catal. Today* **2011,** *172*, (1), 183-188.

33. Wu, G.; Zhang, C.; Li, S.; Han, Z.; Wang, T.; Ma, X.; Gong, J., Hydrogen Production via Glycerol Steam Reforming over Ni/Al_2O_3: Influence of Nickel Precursors. *ACS Sustainable Chem. Eng.* **2013,** *1*, (8), 1052-1062.

34. Appari, S.; Janardhanan, V. M.; Bauri, R.; Jayanti, S.; Deutschmann, O., A detailed kinetic model for biogas steam reforming on Ni and catalyst deactivation due to sulfur poisoning. *Appl. Catal. A-Gen.* **2014,** *471*, 118-125.

35. Shi, F.; Li, Y.; Zhang, Q.; Wang, H.; Dudney, N. J., Preparation of Core/Shell Structured Rutile/Anatase Photocatalyst via Vapor Phase Hydrolysis and its Photocatalytic Degradation of Phenol and Methylene Blue. *J. Am. Ceram. Soc.* **2012,** *95*, (6), 1927-1932.

36. Appari, S.; Janardhanan, V. M.; Bauri, R.; Jayanti, S., Deactivation and regeneration of Ni catalyst during steam reforming of model biogas: An experimental investigation. *Int. J. Hydrogen Energ.* **2014,** *39*, (1), 297-304.

37. Wu, C.; Williams, P. T., A Novel Nano-Ni/SiO_2 Catalyst for Hydrogen Production from Steam Reforming of Ethanol. *Environ. Sci. Technol* **2010,** *44*, 5993-5998.

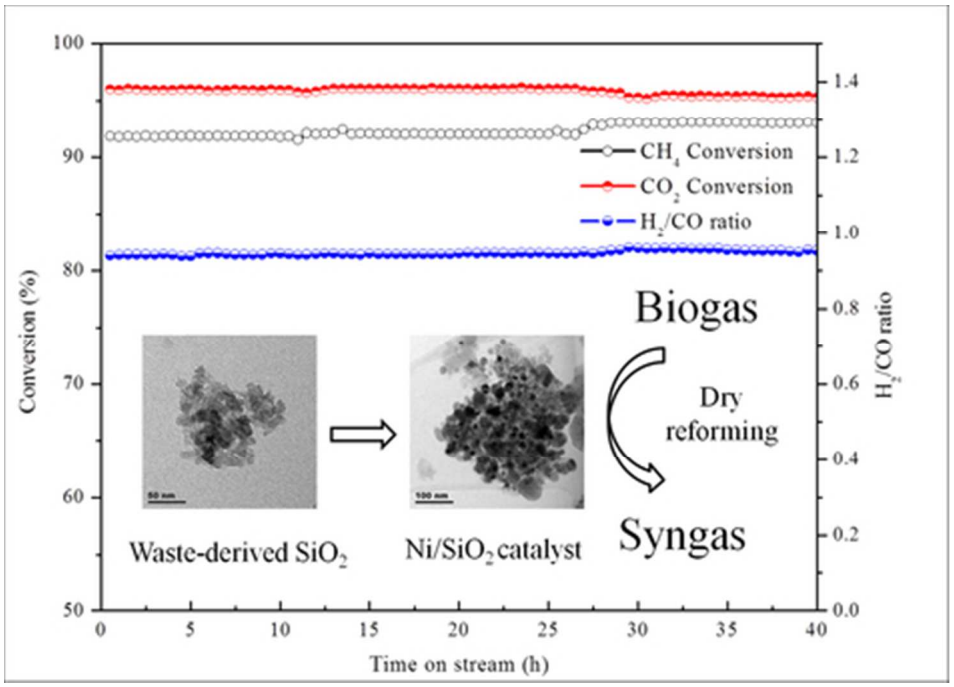

Waste-derived SiO2 was used as catalyst support in biogas dry reforming process, which showed a high catalytic activity and good stability.
39x28mm (300 x 300 DPI)